Materials & Design 223 (2022) 111190

Contents lists available at ScienceDirect

Materials & Design

journal homepage: www.elsevier.com/locate/matdes

Fabrication and characterisation of alumina/aluminium composite materials with a nacre-like micro-layered architecture

Hongbo Wan [a,b], Nathanael Leung [a], Urangua Jargalsaikhan [a], Eric Ho [b], Chaolin Wang [c], Qiang Liu [c], Hua-Xin Peng [d], Bo Su [b], Tan Sui [a,*]

[a] School of Mechanical Engineering Sciences, University of Surrey, Guildford, UK
[b] Biomaterials Engineering Group (bioMEG), Bristol Dental School, University of Bristol, UK
[c] School of Material Science and Engineering, Harbin Institute of Technology (HIT), Harbin, Heilongjiang, China
[d] Institute for Composites Science Innovation (InCSI), School of Materials Science and Engineering, Zhejiang University, Hangzhou, China

HIGHLIGHTS

- The manufacturing of alumina/aluminium composites with nacre-like micro-layered architectures, with ceramic fraction from 18% to 85%, was achieved.
- The composites exhibited superior strength (600 MPa) and fracture toughness (35 MPa.m$^{1/2}$).
- The nacre-like bioinspired composites exhibited significant extrinsic toughening mechanisms.
- This work investigated the effect of interface and microstructure on the mechanical performance.

GRAPHICAL ABSTRACT

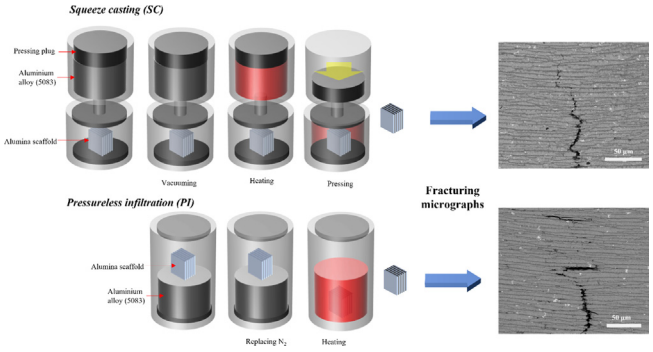

ARTICLE INFO

Article history:
Received 23 May 2022
Revised 20 September 2022
Accepted 21 September 2022
Available online 22 September 2022

Keywords:
Bioinspired
Freeze-casting
Squeeze casting
Pressureless infiltration
Fracture toughness

ABSTRACT

Many natural materials demonstrate ideal design inspirations for the development of lightweight composite materials with excellent damage tolerance. One notable example is the layered architecture of nacre, which possesses toughness an order of magnitude higher than its constituent parts. Man-made nacre-like ceramic/polymer composites obtained through direct infiltration of polymer in ceramic scaffolds have been shown to produce improved mechanical properties over other composite architectures. Replacing the polymer phase with metal could provide higher damage tolerance but the infiltration of metal into complex ceramic scaffolds is difficult due to the surface tension of molten metal. To address this, bioinspired nacre-like micro-layered (μL) alumina scaffolds with different ceramic fractions from 18 to 85% were infiltrated with aluminium alloy 5083 via pressureless and squeeze casting infiltrations techniques. The scaffolds were created using a bi-directional freeze-casting and one-step densification method. As a result, the μL alumina/aluminium composites displayed significant extrinsic toughening mechanisms with both high strength and toughness. The mechanical performance was highly dependent on the interface, microstructure, and composition. The nacre-like composites with 18% alumina and AlN interface displayed a maximum resistance-curve toughness up to around 70 MPa.m^{½} (35 MPa.m^{½} at the ASTM limit) and a flexural strength around 600 MPa.

* Corresponding author.
E-mail address: t.sui@surrey.ac.uk (T. Sui).

https://doi.org/10.1016/j.matdes.2022.111190
0264-1275/

1. Introduction

Current engineering materials for structural applications in the aerospace, energy, and transportation industries are required to maintain stability during their working life in extreme environments and possess low densities in aviation applications. Ceramics are an ideal material, as they are generally stable in extreme environments, due to their strong covalent and ionic bonding. However, the main disadvantage is that they regularly exhibit poor ductility and brittle behaviour, resulting in sudden catastrophic failure. One research topic, for the design of superior composites and structures, is mimicking the architecture of those found in living nature [1]. Nature develops composite materials of mineral and biopolymers with complex hierarchical architectures that exhibit remarkable mechanical properties. Natural nacre found in mollusc shell, is a prominent, well-known example that has a remarkable fracture toughness which is three orders of magnitude higher (in energy terms) than that of its constituents [2,3]. For instance, the nacre found in abalone shell is comprised of aragonite mineral (∼95 vol%) and biopolymer (∼5 vol%), grown into a brick-and-mortar architecture that allows for multiple toughening and strengthening mechanisms to facilitate the creation of damage tolerance. To mimic a nacre-like architecture for engineered materials, ceramic/metal or ceramic/polymer composite materials fabricated via various routines exhibited excellent mechanical properties [1,4–9]. Metal and its alloys are known for being stronger and tougher materials, compared to polymers, from a fracture mechanics perspective. Modelling has also predicted that composite mechanical performance could be enhanced with a metallic compliant phase [10]. Ceramic/metal composites with nacre-like architecture, e.g. brick-and-mortar and lamellar showed apparent higher fracture toughness than analogous ceramic/polymer composites [7,8,11–14]. Apart from brick-and-mortar and lamellar, 'micro-layered (μL)' has been reported to be a novel nacre-like architecture to strengthen and toughen ceramic-based composites [6]. The routine of the bi-directional freeze-casting and one-step densification method were employed to create μL scaffolds. The manufacturing method has the advantages of a shorter processing time, flexibility in controlling the microstructural features, and producing nacre-like μL ceramic scaffolds. The μL exhibits superior mechanical performance than the classic brick-and-mortar architecture in alumina/PMMA system [6], but the freeze-casted μL ceramic scaffold with metal infiltrated composite has yet to be produced and tested. Therefore, the aim of this work is to obtain materials with high strength and damage tolerance by incorporating a metal phase in this novel composite structure.

The composites of ceramic/metal are normally produced by powder metallurgy and molten metal routes. However, it is difficult to generate composites with complex architectures using these methods. Two typical routines are regularly applied to create micro-scale structured ceramic/metal composites, i.e. pressureless (PL) infiltration and squeeze casting (SC) infiltration. The pressureless infiltration process, also known as the Lanxide process, is a cost-effective technique used to penetrate metal into ceramic scaffolds spontaneously without external pressure, where the as-infiltrated metal is adhered to the structure of the scaffolds [15]. This technique is driven by capillary action with the complete absence of external pressure. Therefore, the types of ceramics and metals used are limited, depending on the wettability and capillary forces of ceramic to metal phases. For example, it was reported by Rao *et al.* [16–18] that alumina scaffolds could be infiltrated with an aluminium alloy containing magnesium as the added magnesium decreased the surface tension of the molten alloy, improving the wettability between alumina and aluminium alloy. In contrast, the squeeze casting method uses external pressure to overcome the molten metal surface tension, forcing it to penetrate into the open pores of the ceramic scaffolds [3,19–21]. However, infiltrating metal into ceramic scaffolds with higher ceramic fractions introduces challenges because the higher density produces smaller pores. The small pores resulted in a dramatic increase of the required pressure for full infiltration, which may deform or break the ceramic scaffolds during infiltration. Therefore, a stronger scaffold is needed to withstand the external pressure during the infiltration process [22,23]. Since μL scaffolds exhibit higher compressive strengths (45 MPa) than random porous ceramics (12–24 MPa) due to the stress-transfer effect, this indicates that it would be a good candidate to produce metallic composites via squeeze casting [24,25].

In this work, nacre-like μL alumina scaffolds were prepared via bi-directional freeze-casting/one-step densification with various pore sizes and porosities. Two methods of infiltration, pressureless and squeeze casting, were investigated to infiltrate aluminium alloy 5083 into alumina scaffolds, with ceramic fraction varied between 18% and 85%. The resultant composite materials were mechanically characterised and their toughening mechanisms were discussed.

2. Experimental methodology

2.1. Materials

The raw materials include alumina powder (CT3000SG, Almatis GmbH, Germany), Dolapix CE 64 (ZSCHIMMER&SCHWARZ Germany), polyvinyl alcohol (PVA powder, MW: 30,000–70,000, Sigma Aldrich), octanol-1 (Fisher Scientific), duplication silicone (Elite double 32, Zhermack, UK), paraffin wax (Henry Schein, 900–1514, US), aluminium alloy 5083 (Shropshire stainless and aluminium, UK). The 5083 is an aluminium alloy containing aluminium (∼94%), magnesium (∼4–5%), manganese (∼0.4–1.0%), chromium (∼0.05–0.25%), and other component metals (copper, iron, silicon, titanium, and zinc, ∼1% in total).

2.2. Fabrication of μL alumina scaffolds

The nacre-like μL alumina scaffolds were prepared via bi-directional freeze-casting and one-step densification methods according to our previous work (Fig. 1a) [6]. The ceramic slurries for freeze-casting were prepared by dispersing 10 vol% submicrometric alumina powder into deionised water with the addition of 0.4 wt% of Dolapix, as a dispersant, and 4 wt% of PVA, as a binder, with respect to the ceramic. After 24-hour ball milling, the slurries were de-gassed under vacuum, following the addition of 0.1 ml of octanol. The 10 vol% alumina slurries were then freeze-casted into highly aligned lamellar scaffold ceramic green bodies. The bi-directional freeze-casting mould was composed of a copper base, in the shape of a wedge with a 10° slope, which was covered by a similarly shaped wedge, made of two-part silicone mould rubber, to create a flat surface. To obtain μL alumina scaffolds, the as-obtained highly aligned lamellar ceramic scaffolds were infiltrated with wax and then densified by simple uniaxial pressing, where the ceramic fraction of the resulting μL alumina scaffolds were controlled by the compressive distance of the uniaxial pressing. This relationship between compressive distance and ceramic fraction is illustrated in Fig. 1b. In this work the alumina scaffolds were prepared with different ceramic fractions of 18% (without pressing), 60%, 72%, and 85%, respectively.

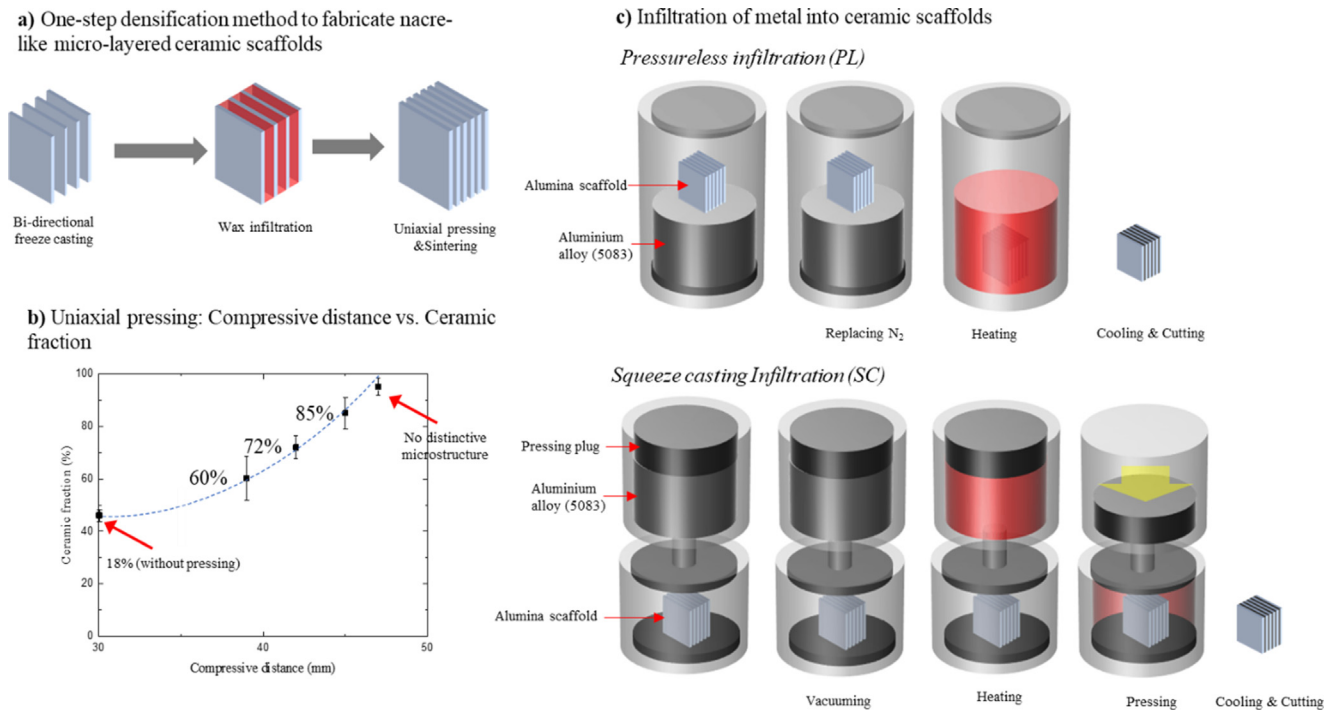

Fig. 1. Schematic diagrams illustrating the fabrication processes of nacre-like alumina/aluminium composites. a) The green body of ceramic scaffolds from bi-directional freeze-casting undergoes one-step densification method to generate the densified ceramic scaffolds with nacre-like architectures. b) The ceramic fraction can be manipulated by varying the compressive distance during uniaxial pressing step. c) The nacre-like ceramic scaffolds were infiltrated with aluminium alloy (5083) via PL infiltration and SC infiltration. (For interpretation of the references to colour in this figure legend, the reader is referred to the web version of this article.)

2.3. Preparation of alumina/aluminium composites

The sintered as-prepared alumina μL scaffolds were then infiltrated with molten aluminium alloy 5083 via two different processing routes, as shown in Fig. 1c: PL infiltration and SC infiltration.

The PL processing route was carried out in a tube furnace, where the alumina scaffold was placed on top of the alloy in a crucible, with the lamellae aligned vertically, as shown in Fig. 1c. Along with the sample, a sacrificial crucible of aluminium powder getter was also placed in the furnace. The furnace was first heated to 400 ℃, at a heating rate of 10 ℃/min, and held there for 60 min to allow the reaction between the getter and oxygen to reduce the possibility of metal oxide forming on the surface of the infiltrating alloy, which would hamper the infiltration process. The tubular furnace was then heated to 950 ℃ and held there for up to 180 min to complete the infiltration.

For the SC processing route, the alumina scaffold was placed in a customised heat-resistant die, the micro-layers of the ceramic scaffold were parallel to the pressing direction, as shown in Fig. 1c. The scaffold and die were preheated to 650 ℃, and held there for 15 min. Subsequently, molten aluminium alloy was poured onto the preheated alumina scaffold and a hydraulic press was then used to apply a uniaxial pressure of 40 MPa for 30 min, allowing the molten aluminium alloy to infiltrate into the alumina scaffold. After the infiltration process, the pressure was maintained until the aluminium alloy was cooled and solidified.

Before further microstructure and mechanical characterisations, samples were grounded using SiC sandpaper from #80 to #2000 finishing and polished using a cloth disk (MD-Nap, Struers, Denmark) with diamond paste (1 μm) to obtain a polished surface. In this work, the prepared μL alumina/aluminium composites were named after their ceramic fraction and manufacturing method. For example, the composite with 18% ceramic fraction prepared via PL is named as 18%-PL.

2.4. Microstructural and composition characterisation

The microstructures of the materials were imaged using Scanning Electron Microscopy (SEM, Quanta 200F, FEI, US) in both Secondary Electron (SE) and Back-Scattered Electron (BSE) modes. The composition and elemental distribution were evaluated using Energy-Dispersive X-ray Spectroscopy (EDS, Jeol IT300, US).

2.5. Mechanical characterisation

Flexural strength and flexural modulus of the composites were determined using three-point bending on a Zwick Roell Z1020 universal testing machine. The bending specimens were cut into rectangular beams with dimension (Thickness (B) × Width (W) × Length (L)) of 1.5 mm × 2 mm × 25 mm (with the support span (S) = 12.5 mm).

Fracture toughness, K_{IC}, and R-curve behaviour were measured using three-point bending on single-edged notched bending specimens (SENB). The SENB specimens were prepared with dimensions of 1.5(B) × 3(W) × 20(L) mm (S = 12.5 mm) for K_{IC} and 2.5 (B) × 5 (W) × 25 (L) mm (S = 20 mm) for R-curve testing, respectively, with the lamellae oriented perpendicularly to the loading direction. A notch was cut in the middle, using a low-speed diamond saw, to a length of a = 0.5 W, where a was 1.5 mm and 2.5 mm and the W was 3 mm and 5 mm for K_{IC} and R-curve measurements. The notch was then sharpened using a custom notching machine, where a razor blade was passed across the notch tip at a speed of 3 Hz, under a 10 N load, whilst being irrigated with a 1 μm diamond suspension (DiaPro Largo3, Struers, Denmark), for one hour. The radius of the sharpened notch was about 50 μm and

the depth was about 200 μm. According to the ASTM 1820 standard [26], the K_{IC} is calculated using the following Eqs. (1) & (2):

$$K_{IC} = \frac{PS}{BW^{\frac{3}{2}}} f\left(\frac{a}{w}\right) \tag{1}$$

$$f\left(\frac{a}{W}\right) = \frac{3\left(\frac{a}{W}\right)^{\frac{1}{2}}\left[1.99 - \left(\frac{a}{W}\right)\left(1-\frac{a}{W}\right)\left(2.15 - 3.93\left(\frac{a}{W}\right) + 2.7\left(\frac{a}{W}\right)^2\right)\right]}{2\left(1+2\frac{a}{W}\right)\left(1-\frac{a}{W}\right)^{\frac{3}{2}}} \tag{2}$$

where P is the maximum force during testing (N).

Non-linear fracture mechanics was used to determine the crack-resistance curve (R-curve) behaviour where the strain energy release rate, represented by the J-integral, was measured as a function of crack extension. Fracture toughness, K_J, was then back-calculated from the measured J values using the standard mode I J–K equivalence ($K_J = \sqrt{JE\prime}$), where E' is the Young's modulus of the composites obtained from the rule of mixtures (RoM).

R-curve tests were performed *in situ* in an SEM (Tescan Mira II, Brno, Czechia) so that the crack propagation could be monitored and recorded. The tests were conducted using a Deben Microtest stage (Deben, UK) with a 150 N load cell and a loading rate of 0.02 mm/min, collecting measurements for at least three samples in each group [6, 20, 21].

In accordance with the ASTM E1820 standard E1820 [26], the J-integral was composed of both elastic and plastic component as shown in Eqs.3&4.

$$J = J_{el} + J_{pl} \tag{3}$$

$$J_{el} = \frac{Kel^2}{E\prime} \tag{4}$$

Using the load P and specimen dimensions, the mode I stress-intensity factor was calculated as Eqs.5&6:

$$K_{el} = \frac{PS}{BW^{\frac{3}{2}}} f\left(\frac{a}{w}\right) \tag{5}$$

$$f\left(\frac{a}{W}\right) = \frac{3\left(\frac{a}{w}\right)^{\frac{1}{2}}\left[1.99 - \left(\frac{a}{w}\right)\left(1-\frac{a}{w}\right)\left(2.15 - 3.93\left(\frac{a}{w}\right) + 2.7\left(\frac{a}{w}\right)^2\right)\right]}{2\left(1+2\frac{a}{w}\right)\left(1-\frac{a}{w}\right)^{\frac{3}{2}}} \tag{6}$$

Considering the load-displacement, J_{pl} for plastic portion was determined by Eq.7.

$$J_{Pl} = \frac{1.9A_{pl}}{Bb} \tag{7}$$

where b is the length of the uncracked ligament and A_{pl} is the area under the load vs. plastic displacement (V_{pl}) curve. By coupling the decreasing b with the crack propagation, the incremental definition of J_{pl} calculation was obtained using Eq.8.

$$J_{Pl(i)} = \left[J_{pl(i-1)} + \frac{1.9\left(A_{pl(i)} - A_{pl(i-1)}\right)}{b_{(i-1)}B}\right] \times \left[1 - \frac{0.9\left(a_{(i)} - a_{(i-1)}\right)}{b_{(i)}}\right] \tag{8}$$

3. Results and discussion

3.1. Mechanical properties

The mechanical properties of the μL alumina/aluminium composites were markedly related to the ceramic fraction and fabrication methods, as shown in Fig. 2. Except for 85%-PL, the flexural modulus of μL alumina/aluminium composites showed positive correlation to the volume fraction stiff phase (alumina) when the ceramic fraction was raised from 18% to 85%. Nevertheless, both flexural strength and K_{IC} exhibited a negative correlation with the ceramic fraction. The 85%-PL exhibited the poorest mechanical performance with the lowest values of strength, modulus, and toughness.

The alloy of metallic phase (Al 5083) is a commercial alloy widely used in car manufacturing, ship building, and pressure vessels owing to its excellent mechanical properties. Here, all well-infiltrated composites (except the 85%-PL) displayed a better strength-toughness combination than the Al 5083 alone [27]. From Fig. 2a, with the addition of the alumina ceramic phase, all composites exhibited higher modulus than Al 5083 (71 GPa) alone [14], which opens possibility of application in high-stiffness engineering components, such as aerospace. The flexural modulus of PL composites was 149 GPa at the ceramic fraction of 18%, and this increased to 251 GPa when the ceramic fraction increased to 72% but dropped to 75 GPa at 85%. For the composites manufactured using SC, the modulus steadily increased from 100 GPa to 220 GPa as the ceramic fraction was raised from 18% to 85%. The moduli of the SC samples were comparable to the RoM, nearly at the mid-point between the upper/lower boundaries of the theoretical RoM, but were lower than the moduli of the samples manufactured using PL. As shown from Fig. 2b, when the ceramic fraction increased from 18% to 85%, the flexural strength of PL composites

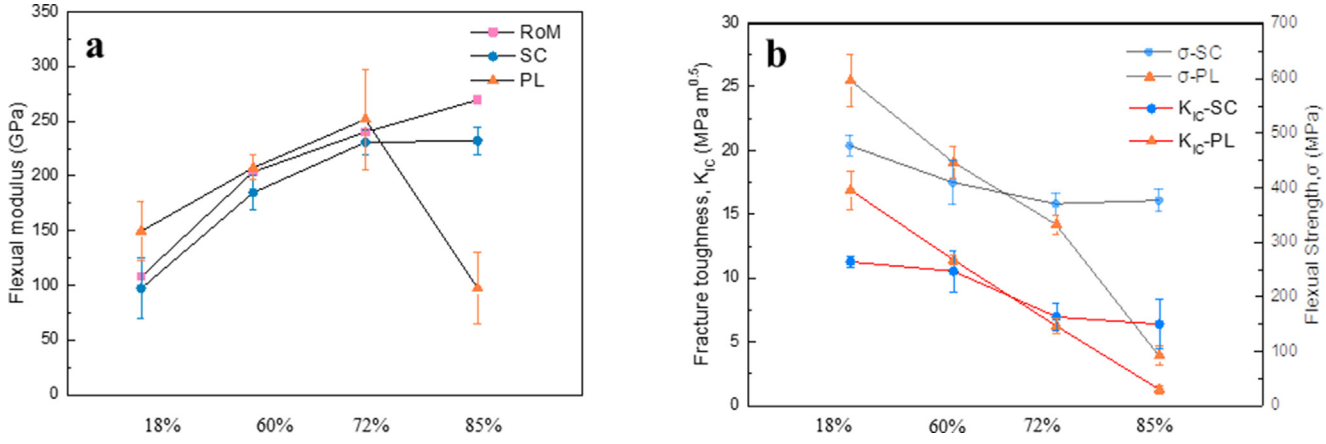

Fig. 2. Mechanical properties including flexural strength, flexural modulus, and K_{IC} of the μL alumina/aluminium composite materials. a) The variation of flexural modulus of composites obtained from stress–strain curves of three-point bending tests as ceramic fraction. Comparably, modulus of composites calculated from the mid-point of RoM was included; b) Effects of ceramic fraction on flexural strength and K_{IC}.

dropped dramatically from 596 MPa to 100 MPa, whilst the SC composites only showed a slight decrease from 450 MPa to 400 MPa. The K_{IC} demonstrated a similar trend as the flexural strength where the PL and SC composites decreased from 17.5 MPa.m$^{1/2}$ to 2.1 MPa.m$^{1/2}$, and 12 MPa.m$^{1/2}$ to 7.5 MPa.m$^{1/2}$, respectively.

Fig. 3 demonstrated the microstructure of μL alumina/aluminium composites with two different infiltration methods (PL and SC) and various ceramic fractions in the range of 18%-85%. It can be seen that the aluminium alloy infiltrated the ceramic scaffolds without damaging the μL architecture of scaffolds for all samples. All the μL composites showed similar wall thicknesses at around 8 μm owing to the bi-directional freeze-casting/densification process [6]. The microstructure of ceramic/metal composites with brick-and-mortar architecture prepared via bottom-up process of ceramic platelets showed higher similarity to natural nacre [8,11–13,28]. However, the production of bulk materials was restricted by expensive processing methods and raw materials, such as hot pressing, spark-plasma sintering and use of alumina platelets. Co-extrusion was also reported to prepare ceramic/metal composites with brick-and-mortar architecture, which displayed similar strengthening and toughening mechanisms, but the expensive raw materials and hot pressing were still needed [29]. In addition to the brick-and-mortar structured composites, lamellar composites created via freeze casting was also discussed [7,28]. The lamellar structure created by freeze casting is ordered in one direction due to ice nucleation of the crystal growth during fabrication, which is difficult to densify with subsequent axial pressing. The ceramic fraction can only be improved by increasing the solid loading of the ceramic suspension. However, this will result in an altered microstructure [20]. The composites with μL architecture in this work is ordered in two-directions, providing flexibility to alter the ceramic fraction from 18% to 85% (Fig. 1), via direct axial pressing, without changing the microstructure.

However, various degrees of porous inclusions due to incomplete infiltration can also be seen. For PL composites, the excellent wettability allowed spontaneous infiltration of the nacre-like alumina scaffolds at very rapid rates without the need for applied pressure, but more and larger defects were observed when the aluminium infiltrated scaffolds with higher ceramic fractions. he 85%-PL composites contain many large unfilled pores, as seen from the SEM images, which indicates that the molten aluminium failed to fully infiltrate into the alumina scaffold due to smaller spacing between ceramic layers, resulting in poor mechanical properties. The SC composites exhibited obvious nacre-like architecture which indicates that the external uniaxial pressing of 40 MPa, during the SC routine, allowed the molten aluminium alloys to penetrate into the open pores of the alumina scaffolds.

The main reason for the mechanical and microstructural variety is the reactive infiltration process of PL in different alumina scaffolds in N_2 atmosphere. As reported before, PL infiltration of aluminium alloy was dependent on the reactions between Mg, N_2, and Al [16]. The Mg in the alloy partially evaporated and reacted with N_2 to form a layer of Mg_3N_2 on the surface of the ceramic scaffolds. This Mg_3N_2 layer then reacted with the molten Al through a substitution reaction producing Mg and AlN:

$$3\ Mg + N_2 = Mg_3N_2 \quad (9)$$

$$Mg_3N_2 + 2Al = 3\ Mg + 2AlN. \quad (10)$$

The metal Mg participated in a chain reaction with N_2 and the produced AlN layer possesses better wettability with the molten aluminium oxide surface layer. By combining the two reactions above, the Mg acted as a catalyst:

$$2Al + N_2 = 2AlN \quad (11)$$

Fig. 3 showed that composites with higher ceramic fractions have relatively more and larger defects at the interface, which was probably because of the different extent of reactions and metal oxide formations during the infiltration process. Obviously, higher ceramic fractions mean narrower spacings between the layers and a smaller contact area between the molten aluminium alloy front and N_2 in the ceramic scaffolds. The chances of N_2 reacting with molten Al to form AlN were thus lower, which was less likely to improve the wetting and facilitation of the Al infiltration. Also, narrower spacings and smaller pores in the scaffolds also mean that it

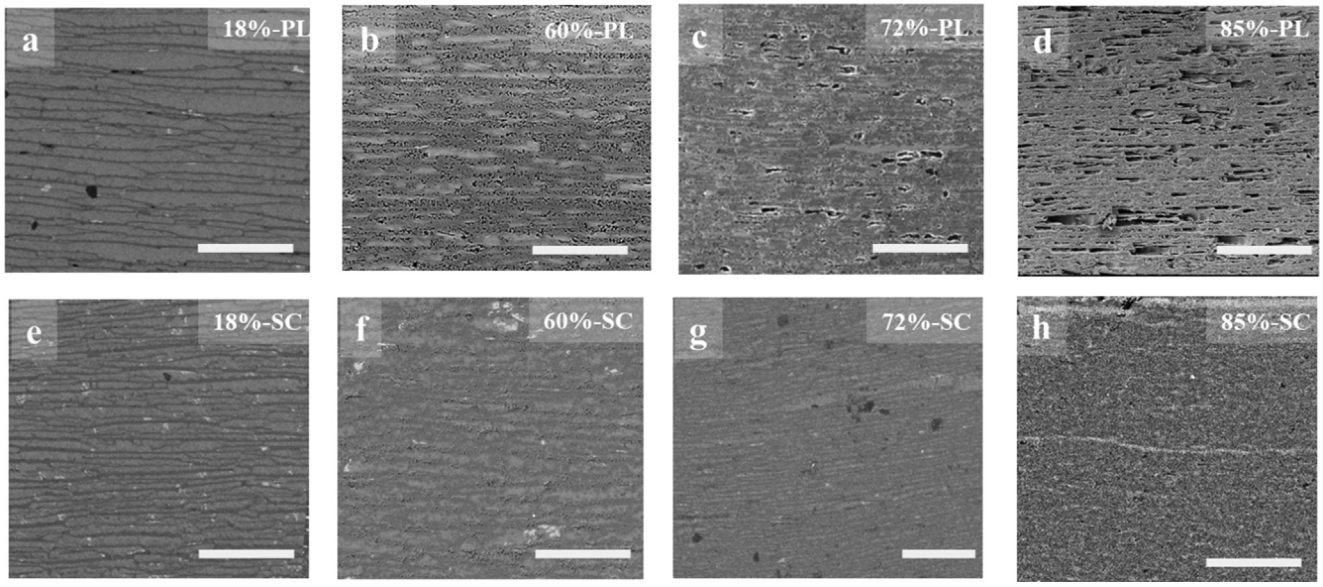

Fig. 3. SEM images showing the microstructures of nacre-like micro-layered (μL) alumina/aluminium composites fabricated in this study. The composites were prepared by PL infiltration and SC infiltration of aluminium into alumina scaffolds with different ceramic fractions from 18% to 85%. a), b), c), and d) are composites prepared by PL with 18%, 60%, 72%, and 85% alumina content, respectively; d), e), f) and g) are composites manufactured via SC with 18%, 60%, 72%, and 85% alumina content, respectively. In all images, the ceramic and the metal appear as the dark and the bright phases respectively. Scale bars: 100 μm.

was more difficult to completely replace the air with N_2 when the tubular furnace was flowed with N_2 before PL infiltration. In the following infiltration process, there was a higher possibility of metal oxide forming from reactions with absorbed air. The as-generated aluminium oxide on the surface of the molten aluminium alloy front was likely to prevent the infiltration process. Hence, at higher ceramic fractions, the obtained composites contained more defects and larger flaws at the interface due to relatively poorer wettability and formation of metal oxide.

As shown in Fig. 2, at 18% and 60% ceramic fractions, the PL composites were stronger, stiffer, and tougher (K_{IC}) than the SC composites and RoM expectation. The SC composites were fabricated under vacuum which means the reaction of N_2 forming an AlN interface was unlikely to occur during infiltration. Therefore, it could be seen that AlN played an important role in strengthening the interface, resulting in better mechanical properties, i.e stiffness, strength and K_{IC}. However, the PL infiltration process also introduced defects at higher ceramic fractions, which resulted in poorer mechanical properties. As the ceramic fraction was raised to 72%, although the modulus of 72%-PL was still slightly higher, the strength and K_{IC} displayed lower values compared to RoM and SC samples. In this case, the strengthening of the interface had a more significant influence on mechanics. At 85%-PL, the aluminium alloy rarely infiltrated into the alumina scaffolds indicating scaffold-like structure where the mechanical properties were attributed to the weakening of defects. Therefore, the 85%-PL was not only weaker and softer but also less resistant the crack initiation.

3.2. R-curve

The *R*-curves, illustrated in Fig. 4, show the resistance to crack propagation in terms of K_J, as a function of crack extension. Fig. 4a compares the *R*-curve behaviour of PL and SC composites with 18% ceramic fractions. It is clear that 18%-PL samples exhibited a rising *R*-curve and stable crack growth with crack extensions of roughly 1.7 mm. The K_J reached approximately 35 MPa.m$^{1/2}$ at the ASTM limit (crack extension = 0.625 mm), but the crack did extend further to 1.7 mm, achieving a high value of $K_J \approx 75$ MPa.m$^{1/2}$. In contrast, the 18%-SC samples displayed a rising *R*-curve behaviour with the fracture toughness increasing from the intersect of the blunting line to approximately 22 MPa.m$^{1/2}$ after 0.625 mm of stable crack growth, and eventually achieving a value as high as 55 MPa.m$^{1/2}$. Overall, this shows that the 18%-PL demonstrated higher K_J from crack initiation to failure, indicating a higher capability of impeding crack propagation.

The PL samples with relatively high ceramic fractions (60%, 72%, and 85%) failed catastrophically without stable crack growth. Incomplete wetting/infiltration of PL infiltration and resultant presence of defects within the composites with higher ceramic fractions are believed to attribute to their deteriorated mechanical properties. Therefore, to eliminate the effect of interface and defects and discuss the relationship between ceramic fraction and toughening, the *R*-curves of SC composites were displayed in Fig. 4b. Apparently, all composites fabricated using SC infiltration displayed stable rising *R*-curve behaviour (Fig. 4b). From the *R*-curves for the SC series composites, the 18%-SC samples obtained the highest values of fracture toughness, reaching a (steady-state) value of approximately 55 MPa.m$^{1/2}$ after 2 mm of crack extension. The 60%-SC showed a lower fracture toughness of 25 MPa.m$^{1/2}$, after 1.5 mm of crack extension. When the ceramic fraction was increased to 72%, the composites showed significantly less stable growth before critical fracture, with a maximum K_J of 22 MPa.m$^{1/2}$, when the crack extended to 0.625 mm. The 85%-SC composites reached a similar K_J of 25 MPa.m$^{1/2}$, but were able to reach a longer crack extension of 2 mm.

3.3. Toughening mechanisms

Stable crack propagation during the *R*-curve measurements offers opportunities to investigate the toughening mechanisms and their relationship to the characteristic microstructural features. The crack in this composite was observed using *in situ* SEM and the micrographs are shown in Fig. 5 and Fig. 6. The path of cracking displayed a remarkable efficiency of the composite structure in resisting crack growth.

Fig. 5 revealed that both 18%-PL and 18%-SC composites samples failed with multiple crack-path deviations off the plane of maximum tensile stress caused by crack deflections along the ceramic/metal interfaces. Thus, both composites obtained raising *R*-curves in which the toughness increases with crack extension. One of the most significant toughening mechanisms is ductile-ligament crack bridging, where the unbroken metal layers span the wake of the crack, and then pull-out (Fig. 5a and c). The unbroken metal toughens the composites by resisting the crack-opening

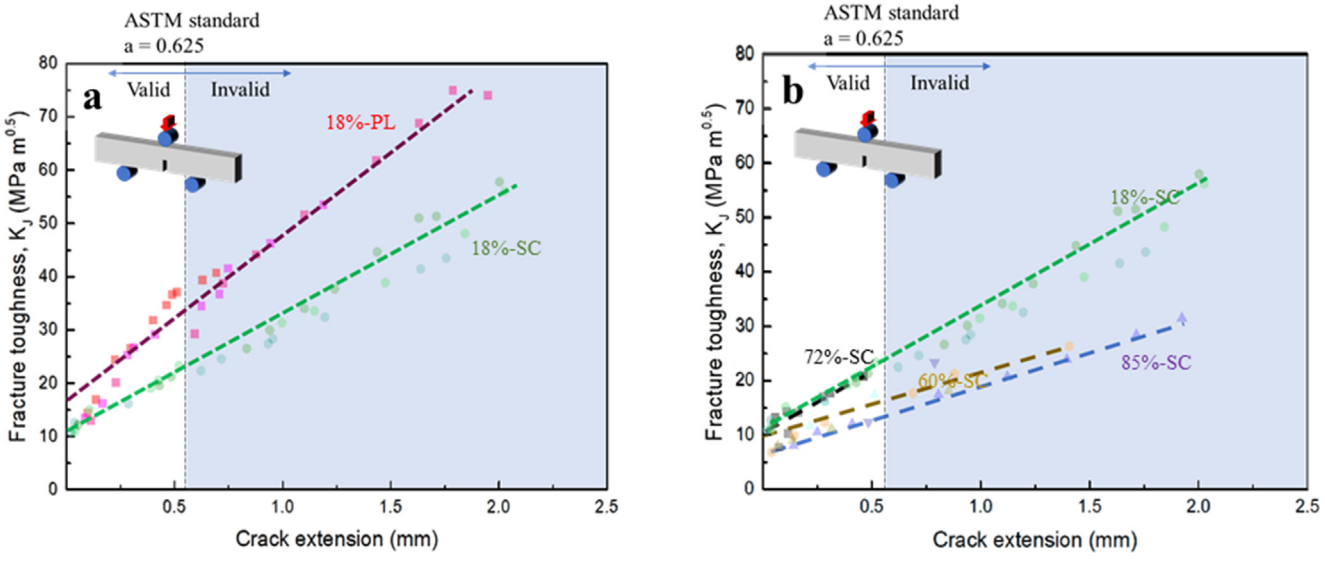

Fig. 4. Fracture toughness *R*-curves of 18%-PL and 18%-SC composites; b) The *R*-curves of composites with various ceramic fractions prepared by SC infiltration.

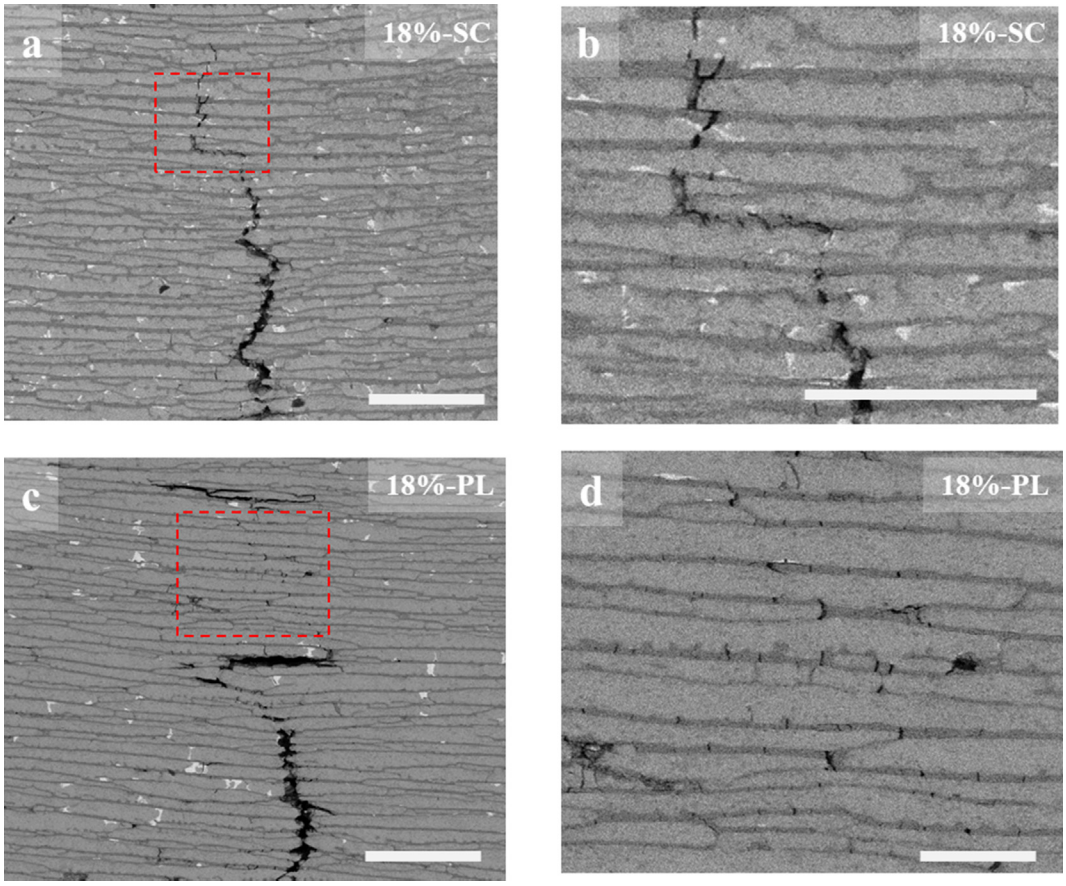

Fig. 5. SEM images taken after *in situ* mechanical testing illustrating crack propagation in the 18%-SC and 18%-PL composite materials. The crack propagations show typical toughening mechanisms: crack deflection, micro-crack, crack bridging, delamination. A) and b) crack propagation in the 18%-SC composites; c) and d) crack propagation in 18%-PL composites. Scale bar for a) and c): 100 μm; for b) and d):50 μm.

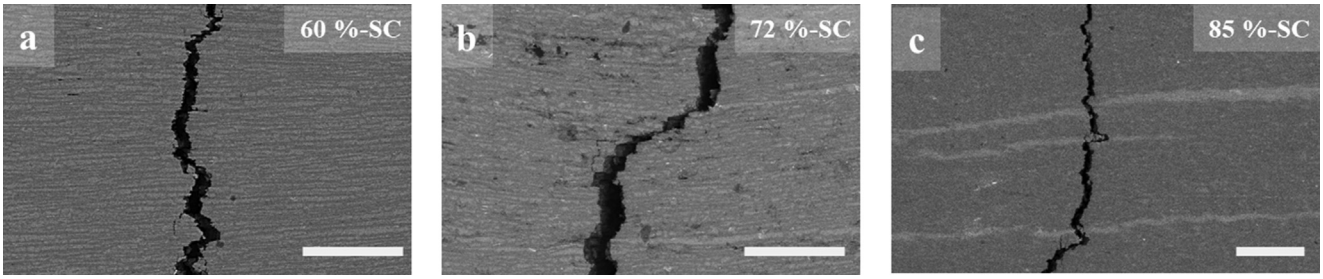

Fig. 6. SEM images illustrating crack propagation in the composite materials with relatively higher ceramic fraction (60–85%) fabricated via SC infiltration. The crack propagation behaviour varies when the ceramic fraction increases. A), b) and c) are 60% and 72% and 85% ceramic fraction respectively. Scale bar: 100 μm.

displacement. When the metal ligaments finally broke, the ceramic began to pull out from the metal phase, causing frictional sliding which dissipated strain energy. Additionally, the 'multiple cracking' fracture mode also contributed to the crack resistance which occurred in the 18%-PL composite (Fig. 5d). As the greater damage distribution and higher energy absorption, the multiple cracking acts to lower crack-tip stresses resulting in higher toughness [30]. Comparably, the 18%-SC composites (Fig. 5b) showed more delamination rather than multiple cracking, which implies that there is a weaker interface in the composites fabricated using SC. The crack transfer from single to multiple mode is because of the plasticity of the metal and the scale of the microstructure and the properties of the metal/ceramic interface [28,30]. Besides the crack mode, the impact of interfacial strength was also significant. Interfacial strength was known to play a key role in the toughening of nacre-like ceramic/polymer composites. Askarinejad *et al.* indicated that for a multi-layered structure, the ideal failure scenario is when the interfaces fail ahead of the fracture of the ceramic layers, which will quickly diminish the strength of the composite [9]. It is obvious that the horizontal interfaces in 18%-PL (Fig. 5) failed with intact ceramic layers, demonstrating interface-leading cracking, which resulted in a higher resistance to crack propagation. These features account for a stronger interface as well as better stress transfer between layers as supported by the higher ultimate flexural strength/modulus and fracture toughness of the PL composites compared to the SC composites.

The composites prepared via SC displayed obvious crack deflection where the crack extension could be captured by SEM during *in situ* testing to plot *R*-curves. The 18%-SC composite obtained the 'valid' toughness of 22 MPa.m$^{1/2}$ and highest value of tough-

ness of ~55 MPa.m$^{1/2}$. This is because the most significant toughening mechanism of crack deflection was not apparent in other composites with high ceramic fractions (see Fig. 6 a-c). Modelling is an effective way to calculate analytically the toughening mechanism in nacre-like ceramic/polymer [9] or ceramic/metal composites [31]. Based on the theoretical modelling of a ceramic/metal system, Huang *et al.* predicted that the metal layer should be at least more than 2.5 times thicker than the ceramic layer for multiple cracking to occur. In the present work, the μL composites with 18% ceramic fraction obtained a metal/ceramic layer thickness ratio of ~4.5. When the ceramic fraction was increased from 60% to 85%, the metal/ceramic layer thickness ratio varied from 0.67 to 0.18. When the ceramic fraction was increased from 18% to 60%, the metal content halved from ~82% to ~40%, reducing the ability of the metallic phase to act as ductile ligaments. In this case, the crack propagation of high ceramic fraction composites only demonstrated other classic toughening mechanisms of layer-by-layer structures similar to ceramic/polymer system [14]: crack deflection, pull-out, and layer-sliding, hence the 60%-SC composite demonstrated a relatively lower fracture toughness. For the 72%-SC composite, the distance between ceramic layers decreases so the metal phase acts not only as a ductile phase but also as a lubricant between the ceramic layers, introducing an extra toughening mechanism: ceramic-ceramic layer frictional sliding. The ceramic-ceramic sliding leads to more energy dissipation, improving the crack resistance which is expressed as a steeper slope in the *R*-curve. This is the significant toughening mechanism in natural nacre [32], and other nacre-like composites when the ceramic fraction is relatively high [3,6,33,34]. However, this structure shows significantly less stable crack growth before critical fracture, K_J = 22-MPa.m$^{1/2}$ after approximately 0.6 mm of crack extension, and this behaviour can be explained by the 'loss' of ductility due to the low content of metal phase. In the 85%-SC composite, the ceramic layers were much closer and even fused together to form massive ceramic bridges in which most metal layers lost their continuity and functions [6], i.e., acting as neither a load-bearing phase nor a lubricant, hence the crack went through tens of layers easily, displaying a low initiation fracture toughness (~6 MPa.m$^{1/2}$) in the *R*-curve. However, the crack blunting and deflecting near the thick metal layer was observed as a significant toughening mechanism in 85%-SC. There are a few relatively thicker metallic layers generated during the densification process and the metal layer stabilised the crack in the composite. Therefore, although the 85%-SC also displayed lower fracture toughness at 6 MPa.m$^{1/2}$ according to ASTM standard, the crack further propagated to 1.8 mm with a fracture toughness at ~26 MPa.m$^{1/2}$.

4. Conclusion

The nacre-like μL alumina/aluminium composites were prepared by infiltrating molten metal into ceramic scaffolds using bi-directional freeze-casting with ceramic fractions from 18% to 85%. The infiltration methods of PL infiltration and SC infiltration played a key role in manipulating the interface, microstructure, and mechanical properties. The molten aluminium can be infiltrated into the ceramic scaffolds with low ceramic fractions without applied pressure or under an external pressure of 40 MPa without damaging the μL alumina scaffolds. Herein the μL architecture of the composites exhibited promising mechanical properties that were attributed to multiple toughening mechanisms including crack deflection, pull-out, crack bridging, and multiple cracking. The 18%-PL displayed a remarkable mechanical combination of flexural strength (600 MPa) and fracture toughness (35 MPa.m$^{1/2}$), due to a strong AlN interface, resulting in multiple cracking in ceramic layers. However, the reaction to form AlN also impeded the infiltration process for ceramic scaffolds with high ceramic fractions (60%-85%), leading to the formation of defects at the interface with negative impact to mechanical performance of the resultant composites. The SC alumina/aluminium composites with ceramic fraction from 18% to 85% displayed significant multiple toughening mechanisms. Therefore, it is more suitable to prepare μL composite materials even with very high ceramic fractions.

Declaration of Competing Interest

The authors declare that they have no known competing financial interests or personal relationships that could have appeared to influence the work reported in this paper.

Acknowledgements

This work was supported by the Engineering and Physical Sciences Research Council (EPSRC) project (EP/S022813/1).

References

[1] C. Ortiz, M.C. Boyce, Bioinspired Structural Materials, Science 319 (5866) (2008) 1053–1054.
[2] M.A. Meyers, P.-Y. Chen, A.-Y.-M. Lin, Y. Seki, Biological materials: structure and mechanical properties, Prog. Mater. Sci. 53 (1) (2008) 1–206.
[3] F. Barthelat, D. Zhu, A novel biomimetic material duplicating the structure and mechanics of natural nacre, J. Mater. Res. 26 (10) (2011) 1203–1215.
[4] H. Bai, Y. Chen, B. Delattre, A.P. Tomsia, R.O. Ritchie, Bioinspired large-scale aligned porous materials assembled with dual temperature gradients, Sci. Adv. 1 (11) (2015).
[5] M.E. Launey, E. Munch, D.H. Alsem, H.B. Barth, E. Saiz, A.P. Tomsia, R.O. Ritchie, Designing highly toughened hybrid composites through nature-inspired hierarchical complexity, Acta Mater. 57 (10) (2009) 2919–2932.
[6] H. Wan, N. Leung, S. Algharaibeh, T. Sui, Q. Liu, H.-X. Peng, B. Su, Cost-effective fabrication of bio-inspired nacre-like composite materials with high strength and toughness, Compos. B Eng. 202 (2020) 108414.
[7] M.E. Launey, E. Munch, D.H. Alsem, E. Saiz, A.P. Tomsia, R.O. Ritchie, A novel biomimetic approach to the design of high-performance ceramic-metal composites, J. R. Soc. Interface 7 (46) (2010) 741–753.
[8] J. Huang, S. Daryadel, M. Minary-Jolandan, Low-Cost Manufacturing of Metal-Ceramic Composites through Electrodeposition of Metal into Ceramic Scaffold, ACS Appl. Mater. Interfaces 11 (4) (2019) 4364–4372.
[9] S. Askarinejad, N. Rahbar, Mechanics of bioinspired lamellar structured ceramic/polymer composites: Experiments and models, Int. J. Plast. 107 (2018) 122–149.
[10] M.R. Begley, N.R. Philips, B.G. Compton, D.V. Wilbrink, R.O. Ritchie, M. Utz, Micromechanical models to guide the development of synthetic 'brick and mortar' composites, J. Mech. Phys. Solids 60 (8) (2012) 1545–1560.
[11] A. Wat, C. Ferraro, X. Deng, A. Sweet, A.P. Tomsia, E. Saiz, R.O. Ritchie, Bioinspired Nacre-Like Alumina with a Metallic Nickel Compliant Phase Fabricated by Spark-Plasma Sintering, Small 15 (31) (2019) 1900573.
[12] J. Huang, W.S. Rubink, H. Lide, T.W. Scharf, R. Banerjee, M. Minary-Jolandan, Alumina-Nickel Composite Processed via Co-Assembly Using Freeze-Casting and Spark Plasma Sintering, Adv. Eng. Mater. 21 (3) (2019) 1801103.
[13] E. Poloni, F. Bouville, C.H. Dreimol, T.P. Niebel, T. Weber, A.R. Biedermann, A.M. Hirt, A.R. Studart, Tough metal-ceramic composites with multifunctional nacre-like architecture, Sci. Rep. 11 (1) (2021) 1621.
[14] S. KumarSingh, R. Mohan Tiwari, A. kumar, S. Kumar, QasimMurtaza, S. Kumar, Mechanical Properties and Micrstructure of Al-5083 by TIG, Materials Today: Proceedings 5(1, Part 1) (2018) 819-822.
[15] A.W. Urquhart, Novel reinforced ceramics and metals: a review of Lanxide's composite technologies, Mater. Sci. Eng., A 144 (1) (1991) 75–82.
[16] B.S. Rao, V. Jayaram, New technique for pressureless infiltration of Al alloys into Al2O3 preforms, J. Mater. Res. 16 (10) (2001) 2906–2913.
[17] A. Klinter, G. Mendoza-Suarez, R. Drew, Wetting of Pure Aluminum and Selected Alloys on Polycrystalline Alumina and Sapphire, Materials Science and Engineering A-structural Materials Properties Microstructure and Processing - MATER SCI ENG A-STRUCT MATER 495 (2008) 147–152.
[18] A. Sangghaleh, M. Halali, Effect of magnesium addition on the wetting of alumina by aluminium, Appl. Surf. Sci. 255 (19) (2009) 8202–8206.
[19] S. Roy, A. Wanner, Metal/ceramic composites from freeze-cast ceramic preforms: Domain structure and elastic properties, Compos. Sci. Technol. 68 (5) (2008) 1136–1143.
[20] Y. Wang, P. Shen, R.-F. Guo, Z. Hu, Q.-C. Jiang, Developing high toughness and strength Al/TiC composites using ice-templating and pressure infiltration, Ceram. Int. 43 (2016).

[21] Q. Liu, F. Ye, Y. Gao, S. Liu, H. Yang, Z. Zhou, Fabrication of a new SiC/2024Al co-continuous composite with lamellar microstructure and high mechanical properties, J. Alloy. Compd. 585 (2014) 146–153.
[22] C. Garcia-Cordovilla, E. Louis, J. Narciso, Pressure infiltration of packed ceramic particulates by liquid metals, Acta Mater. 47 (18) (1999) 4461–4479.
[23] A. Mattern, B. Huchler, D. Staudenecker, R. Oberacker, A. Nagel, M.J. Hoffmann, Preparation of interpenetrating ceramic–metal composites, J. Eur. Ceram. Soc. 24 (12) (2004) 3399–3408.
[24] S.W.A.R. Algharaibeh, Fabrication and characterisation of biomimetic nacre-like ceramic/polymer composite a potential CAD/CAM dental material Algharaibeh, Student thesis: Doctoral Thesis › Doctor of Philosophy (PhD) (2020).
[25] I. Sabree, J.E. Gough, B. Derby, Mechanical properties of porous ceramic scaffolds: Influence of internal dimensions, Ceram. Int. 41 (7) (2015) 8425–8432.
[26] Standard Test Method for Measurement of Fracture Toughness.
[27] R.L. Tobler, R.P. Reed, Fracture Mechanics Parameters for a 5083–0 Aluminum Alloy at Low Temperatures, J. Eng. Mater. Technol. 99 (4) (1977) 306–312.
[28] C. Ferraro, S. Meille, J. Réthoré, N. Ni, J. Chevalier, E. Saiz, Strong and tough metal/ceramic micro-laminates, Acta Mater. 144 (2018) 202–215.
[29] R.P. Wilkerson, B. Gludovatz, J. Watts, A.P. Tomsia, G.E. Hilmas, R.O. Ritchie, A Novel Approach to Developing Biomimetic (“Nacre-Like”) Metal-Compliant-Phase (Nickel–Alumina) Ceramics through Coextrusion, Adv. Mater. 28 (45) (2016) 10061–10067.
[30] K.L. Hwu, B. Derby, Fracture of metal/ceramic laminates—I. Transition from single to multiple cracking, Acta Materialia 47 (2) (1999) 529–543.
[31] Y. Huang, H. Zhang, The role of metal plasticity and interfacial strength in the cracking of metal/ceramic laminates, Acta Metall. Mater. 43 (4) (1995) 1523–1530.
[32] F. Barthelat, H. Tang, P.D. Zavattieri, C.M. Li, H.D. Espinosa, On the mechanics of mother-of-pearl: A key feature in the material hierarchical structure, J. Mech. Phys. Solids 55 (2) (2007) 306–337.
[33] Z. Yin, F. Hannard, F. Barthelat, Impact-resistant nacre-like transparent materials, Science 364 (6447) (2019) 1260.
[34] K.C. Datsiou, Bioinspired improvement of laminated glass, Science 364 (6447) (2019) 1232.